

TEMPORALLY-SHAPED ULTRAVIOLET PULSES FOR TAILORED BUNCH GENERATION AT ARGONNE WAKEFIELD ACCELERATOR

T. Xu^{1*}, R. Lemons², S. Carbajo^{2,3}, P. Piot^{1,4}

¹Northern Illinois University, DeKalb, IL 60115, USA

²SLAC National Accelerator Laboratory, Menlo Park, CA 94025, USA

³University of California, Los Angeles, CA 90095, USA

⁴Argonne National Laboratory, Lemont, IL 60439, USA

Abstract

Photocathode laser shaping is an appealing technique to generate tailored electron bunches due to its versatility and simplicity. Most photocathodes require photon energies exceeding the nominal photon energy produced by the lasing medium. A common setup consists of an infrared (IR) laser system with nonlinear frequency conversion to the ultraviolet (UV). In this work, we present the numerical modeling of a temporal shaping technique capable of producing electron bunches with linearly-ramped current profiles for application to collinear wakefield accelerators. Specifically, we show that controlling higher-order dispersion terms associated with the IR pulse provides some control over the UV temporal shape. Beam dynamics simulation of an electron-bunch shaping experiment at the Argonne Wakefield Accelerator is presented.

INTRODUCTION

Beam-driven collinear wakefield acceleration requires electron bunches with tailored current profiles to achieve higher transformer-ratios [1]. An important class of current profiles consists of linearly-ramped (“triangular”) distributions. Such electron bunch can be obtained by longitudinal beam shaping techniques which often involves multi-stage phase-space manipulation [2–5]. Laser shaping is a simple yet powerful technique that supports photoinjector generation of longitudinally-shaped electron bunches [6, 7]. It directly controls the distribution of electron bunch at photocathode and does not require any modification of the accelerator beamline.

A laser shaping experiment is under preparation at the Argonne Wakefield Accelerator (AWA). Additional diffraction gratings are being installed in the laser system to achieve a recently demonstrated nonlinear shaping technique named dispersion controlled nonlinear shaping (DCNS) pioneered at the Linac Coherent Light Source [8]. Compared with existing laser-shaping method [6, 7], DCNS does not induce significant energy loss of laser pulses and can be scaled to higher repetition rates. In addition, the pulses generated from DCNS are narrowband and have little to no residual spectral phase across the bandwidth so the pulse shapes are not affected by further nonlinear conversion or general dispersion. In this work, we will describe the principle of DCNS and show that temporally shaped UV pulses can be

obtained by modifying the spectral phase of the IR laser pulse. Finally, we discuss the distortion of electron bunch shapes after photoemission and derive a condition for preserving the sharp tails of the triangular profile.

DISPERSION CONTROLLED NONLINEAR SHAPING

The spectral phase of a laser pulse can be expanded in Taylor series [9],

$$\begin{aligned} \varphi(\omega) = & \varphi_0 + \frac{d\varphi}{d\omega}(\omega - \omega_0) + \frac{1}{2} \frac{d^2\varphi}{d\omega^2}(\omega - \omega_0)^2 \\ & + \frac{1}{6} \frac{d^3\varphi}{d\omega^3}(\omega - \omega_0)^3 + \dots + \frac{1}{n!} \frac{d^n\varphi}{d\omega^n}(\omega - \omega_0)^n \end{aligned} \quad (1)$$

here φ_0 and $d\varphi/d\omega$ are carrier-envelope phase and group delay and neither has any effect on the pulse shape. The second order dispersion (SOD) term, $d^2\varphi/d\omega^2$, also known as *chirp*, results in a group delay linearly dependent on the frequency for each frequency component and stretch the pulse length. The third order dispersion (TOD) term, $d^3\varphi/d\omega^3$ results in a group delay quadratically dependent on frequency,

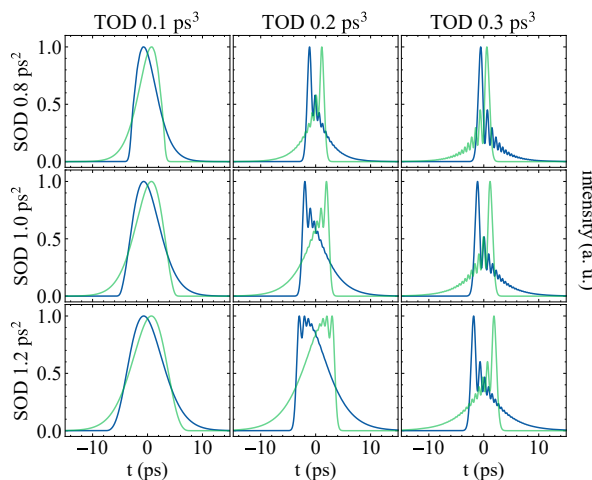


Figure 1: Intensity profile for a pulse with different values of SOD and TOD. Each row has the same magnitude of SOD and each column has the same magnitude of TOD. The blue traces show the intensity profile for a negative SOD and positive TOD while the green traces are for pulses with positive SOD and negative TOD. The intensities are in arbitrary units.

* xu@niu.edu

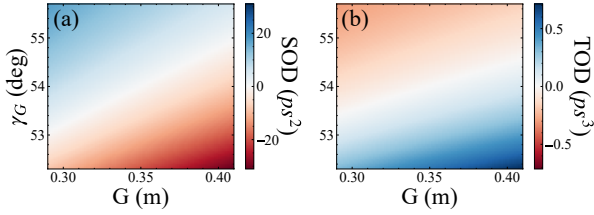


Figure 2: Additional SOD (a) and TOD (b) introduced by the grating compressor when (G, γ_G) is detuned from nominal setup (0.35 m, 54 deg).

so frequencies on both sides of central frequency, $\omega_0 \pm \delta\omega$, overlap in time and create beating in intensity. Pulses with TOD have oscillations at the leading or trailing edges of the pulse and the intensity profiles become asymmetric. Normally, SOD and TOD need to be minimized when aiming for very short pulses. For pulse shaping, one can purposely introduce SOD and TOD to the pulse to achieve desired shapes, e.g., triangles. Figure 1 shows the intensity profiles of a transform-limited Gaussian pulse with central wavelength $\lambda_0=785$ nm and FWHM bandwidth $\Delta\lambda = 2$ nm after applying different values of SOD and TOD. With the right combination of SOD and TOD, we can obtain a pulse with a triangular intensity profile and control its orientation with the sign of TOD.

The SOD and TOD of a pulse can be introduced through diffraction gratings. The SOD and TOD introduced by a grating compressor after a single pass are given by [10],

$$\text{SOD} = -\frac{\lambda}{2\pi c^2} \left(\frac{\lambda}{d}\right)^2 \frac{G}{\cos^3(\gamma_G - \theta)} \quad (2a)$$

$$\text{TOD} = -\frac{3\lambda}{2\pi c \cos^2(\gamma_G - \theta)} \left[\cos^2(\gamma_G - \theta) + \frac{\lambda}{d} \sin(\gamma_G - \theta) \right] \text{SOD} \quad (2b)$$

where λ is the laser wavelength, d is the grating constant, G is the perpendicular distance between two gratings, γ_G is the incidence angle of the input beam, and θ is the difference between incident and diffracted angles. Usually, G and γ_G of the grating compressor are set so that the compressor compensates for the dispersion introduced by the stretcher. Detuning from the nominal configuration by varying G and γ_G allows control over SOD and TOD and hence enables shaping of the input pulse; see Fig. 2.

NONLINEAR MIXING

The temporal shaping technique discussed in the previous section mainly applies to IR pulses produced in typical free-space laser systems. In a photoinjector, high-quantum-efficiency photocathodes, such as Cs₂Te, requires IR pulses to be upconverted to UV with nonlinear crystals. We consider the propagation of three pulses in the nonlinear crystal and by convention names the three waves ‘‘pump’’ (p), ‘‘signal’’ (s) and ‘‘idler’’ (i) ($\omega_p = \omega_s + \omega_i$ and $\omega_p > \omega_s > \omega_i$) with their electric fields $E_j(t, z) = A_j(t, z)e^{i(k_j z - \omega_j t)}$. Here

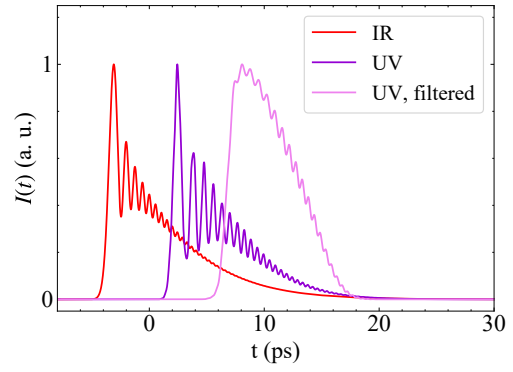


Figure 3: Peak-normalized temporal profiles of the shaped IR pulse (red), UV pulse before (purple), and after (violet) the bandwidth filter.

$A_j(t, z)$ is the field envelope profiles with $j = p, s, i$. Under slowly-varying amplitude approximation ($\left| \frac{d^2 A_j}{dz^2} \right| \ll \left| k_j \frac{dA_j}{dz} \right|$), the evolution of $A_j(t, z)$ can be described by the coupled wave equations [11],

$$\left(\frac{\partial}{\partial z} + \frac{1}{v_{g,i}} \frac{\partial}{\partial t} - i \frac{D_i}{2} \frac{\partial^2}{\partial t^2} \right) A_i(t, z) = \frac{i\omega_i d_{\text{eff}}}{n_i c} A_p(t, z) A_s^*(t, z) e^{i\Delta k z} \equiv P_i(t, z) \quad (3a)$$

$$\left(\frac{\partial}{\partial z} + \frac{1}{v_{g,s}} \frac{\partial}{\partial t} - i \frac{D_s}{2} \frac{\partial^2}{\partial t^2} \right) A_s(t, z) = \frac{i\omega_s d_{\text{eff}}}{n_s c} A_p(t, z) A_i^*(t, z) e^{i\Delta k z} \equiv P_s(t, z) \quad (3b)$$

$$\left(\frac{\partial}{\partial z} + \frac{1}{v_{g,p}} \frac{\partial}{\partial t} - i \frac{D_p}{2} \frac{\partial^2}{\partial t^2} \right) A_p(t, z) = \frac{i\omega_p d_{\text{eff}}}{n_p c} A_s(t, z) A_i(t, z) e^{-i\Delta k z} \equiv P_p(t, z) \quad (3c)$$

where $v_{g,j}$ is the group velocity, $D_j = \frac{\partial}{\partial \omega} \left(\frac{1}{v_{g,j}} \right)_{\omega=\omega_j}$ is the group velocity dispersion, n_j is the refraction index, d_{eff} is the effective second order susceptibility, and $\Delta k = k_p - k_s - k_i$ is the wave vector mismatch. Here the effects of higher-order dispersion, absorption, and spatial walk-off are ignored. Eq. (3a-3c) describe the general case of mixing where the frequencies of the three waves differ. For SHG, $\omega_s = \omega_i$ and $A_s(t, z) = A_i(t, z)$ so the three equations reduces to two.

For arbitrary pulse shapes, analytical solutions do not exist, and we resort to numerical solutions using a split-step Fourier method [11]. We start with an IR pulse with FWHM bandwidth $\Delta\lambda = 2.5$ nm and SOD=1.3 ps², TOD=0.233 ps³ and let it propagate through a 5 mm KDP crystal for SHG. The generated blue pulse is then mixed with a replica of the initial IR pulse in a 1 mm KDP crystal for SFG. Finally, the UV pulse is passed through a 0.2 nm bandwidth filter to remove the oscillation in the temporal profile. Temporal profiles of the initial IR pulse, the generated UV pulse before and after the bandwidth filter appear in Fig. 3. Although the

nonlinear mixing deepens the oscillation in the UV temporal profile, a linearly-ramped, triangular profile can be obtained after the spectral filter.

ELECTRON BEAM DYNAMICS

In photoemission sources, the distribution of emitted electrons initially mirrors the temporal profile of the laser pulse impinged on the cathode. However, at higher bunch charge, the electron bunch current profile can be significantly distorted by image charge close to the photocathode surface and space-charge forces after emission. Here we derive a condition for bunch charge, gun gradient, laser pulse length and spot radius and show that the sharp tail of triangular current profile can be preserved when the condition is satisfied.

The electron bunch length L just after emission can be estimated by [12],

$$L = \sqrt{\left(\frac{mc^2}{eE_{\text{acc}}}\right)^2 + (c\Delta t)^2} - \frac{mc^2}{eE_{\text{acc}}} \quad (4)$$

where Δt is the total emission time, E_{acc} is the accelerating field. Consider a round triangular bunch with a uniform transverse profile and a radius R , the on-axis longitudinal

space charge field is shown in Fig. 4(a). The decelerating field at the tail of the bunch is given by,

$$E_{z,\text{tail}}(R, L') = \frac{Q}{2\pi\epsilon_0 L'^2 R^2} \left[\frac{L'^3 - R^2 L'}{\sqrt{L'^2 + R^2}} - 2RL' - L'^2 + R^2 \ln\left(\frac{R}{\sqrt{L'^2 + R^2} - R}\right) \right] \quad (5)$$

where Q is the charge and $L' = \gamma L$ is the bunch length in its rest frame. Just after photoemission, the energy gain of the bunch is small, so $\gamma \approx 1$ and $L' \approx L$.

The tail of the triangular profile can be preserved if the decelerating field at the tail is negligible compared with the accelerating field,

$$E_{z,\text{self}} + E_{z,\text{image}} \approx 2E_{z,\text{tail}} \ll E_{\text{acc}} \quad (6)$$

here $E_{z,\text{self}}$ and $E_{z,\text{image}}$ are the decelerating field from the bunch itself and the image charge. Figure 4(b) shows the decelerating field at bunch tail for bunches with different laser pulse lengths and spot radius. In the four radius shown, only $R=3$ mm meet the condition above when Δt is between 10-20 ps (the pulse length range obtained in the previous section).

To verify the condition in Eq. (6), we performed IMPACT-T simulation for a 3 nC electron in AWA photoinjector beam-line. The RF gun is a 1.3 GHz $1 + \frac{1}{2}$ resonant cavity operating at $E_0=60$ MV/m and $\phi=60^\circ$ so $E_{\text{acc}}=52$ MV/m. The initial macroparticle distribution are generated corresponding to the four radius in Fig. 4(b) and $\Delta t=13$ ps. The current profiles of the electron bunch after the RF gun are shown in Fig. 4(c). It can be seen only the case with a radius $R=3$ mm maintains the sharp tail in the triangular profile.

CONCLUSION

In conclusion, we have presented the numerical modeling of dispersion controlled nonlinear shaping and showed that a triangular temporal profile can be obtained with SOD and TOD tuning and maintained during nonlinear conversion. We showed that the sharp tail of the triangular profile can be preserved after photoemission if a certain condition is satisfied. The simulation for laser and beam dynamics presented in this work will be used to guide the electron beam shaping experiment at AWA. Ultimately, the laser shaping technique is expected to be integrated with masked-based [13] method to achieve precise longitudinal shapes while maintaining high charge transmission.

ACKNOWLEDGEMENTS

TX and PP are support by the U.S. Department of Energy under contracts DE-SC0022010 to NIU, DE-AC02-06CH11357 with ANL. RL and SC are supported by the U.S. Department of Energy, Office of Science, Office of Basic Energy Sciences under Contracts No. DE-AC02-76SF00515 and DE-SC0022559 to SLAC and UCLA.

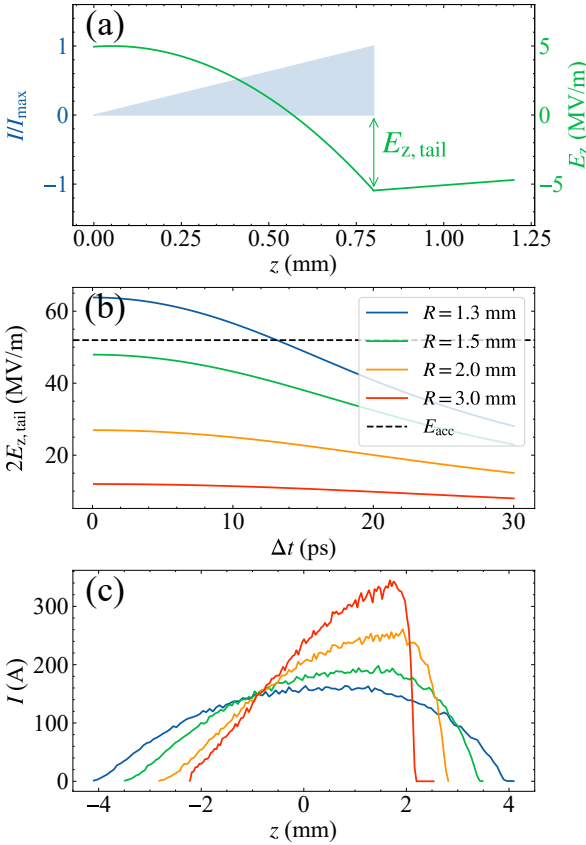


Figure 4: (a) Self field of a triangular bunch in its rest frame. (b) Deceleration field at bunch tail after photoemission. (c) simulated current profiles after RF gun for bunches with different initial spot radius. The colors are the same as the legend in (b). In (a) and (c) bunch head is on the left.

REFERENCES

- [1] K. L. Bane, P. Chen, and P. B. Wilson, "On collinear wake field acceleration," in *Proc. PAC1985*, Vancouver, BC, Canada, May 13-16, 1985, vol. 32, 1985, pp. 3524–3526. doi:10.1109/TNS.1985.4334416
- [2] R. J. England, J. B. Rosenzweig, and G. Travish, "Generation and measurement of relativistic electron bunches characterized by a linearly ramped current profile," *Phys. Rev. Lett.*, vol. 100, no. 21, p. 214 802, 2008. doi:10.1103/PhysRevLett.100.214802
- [3] P. Piot *et al.*, "Generation and characterization of electron bunches with ramped current profiles in a dual-frequency superconducting linear accelerator," *Phys. Rev. Lett.*, vol. 108, no. 3, p. 034 801, 2012. doi:10.1103/PhysRevLett.108.034801
- [4] G. Andonian *et al.*, "Generation of ramped current profiles in relativistic electron beams using wakefields in dielectric structures," *Phys. Rev. Lett.*, vol. 118, no. 5, p. 054 802, 2017. doi:10.1103/PhysRevLett.118.054802
- [5] G. Ha *et al.*, "Precision control of the electron longitudinal bunch shape using an emittance-exchange beam line," *Phys. Rev. Lett.*, vol. 118, no. 10, p. 104 801, 2017. doi:10.1103/PhysRevLett.118.104801
- [6] G. Loisch *et al.*, "Photocathode laser based bunch shaping for high transformer ratio plasma wakefield acceleration," *Nucl. Instrum. Methods Phys. Res., Sect. A*, vol. 909, pp. 107–110, 2018. doi:10.1016/j.nima.2018.02.043
- [7] F. Liu, S. Huang, S. Si, G. Zhao, K. Liu, and S. Zhang, "Generation of picosecond pulses with variable temporal profiles and linear polarization by coherent pulse stacking in a birefringent crystal shaper," *Opt. Express*, vol. 27, no. 2, pp. 1467–1478, 2019. doi:10.1364/OE.27.001467
- [8] R. Lemons, N. Neveu, J. Duris, A. Marinelli, C. Durfee, and S. Carbajo, "Temporal shaping of narrow-band picosecond pulses via noncolinear sum-frequency mixing of dispersion-controlled pulses," *Phys. Rev. Accel. Beams*, vol. 25, no. 1, p. 013 401, 2022. doi:10.1103/PhysRevAccelBeams.25.013401
- [9] A. Monmayrant, S. Weber, and B. Chatel, "A newcomer's guide to ultrashort pulse shaping and characterization," *J. Phys. B: At. Mol. Opt. Phys.*, vol. 43, no. 10, p. 103 001, 2010.
- [10] J.-C. Diels and W. Rudolph, *Ultrashort laser pulse phenomena*. Elsevier, 2006.
- [11] A. V. Smith, R. J. Gehr, and M. S. Bowers, "Numerical models of broad-bandwidth nanosecond optical parametric oscillators," *J. Opt. Soc. Am. B*, vol. 16, no. 4, pp. 609–619, 1999. doi:10.1364/JOSAB.16.000609
- [12] O. J. Luiten, "Beyond the RF Photogun," in *The Physics and Applications of High Brightness Electron Beams*, 2003, pp. 108–126. doi:10.1142/9789812705235_0006
- [13] G. Ha, J. G. Power, J. Shao, M. Conde, and C. Jing, "Coherent synchrotron radiation free longitudinal bunch shaping using transverse deflecting cavities," *Phys. Rev. Accel. Beams*, vol. 23, no. 7, p. 072 803, 2020. doi:10.1103/PhysRevAccelBeams.23.072803